AIMS Mathematics

https://www.aimspress.com/journal/Math

AIMS Mathematics, 11(8): 24928–24957.
DOI: 10.3934/math.20261002
Received: 07 April 2026
Revised: 27 July 2026
Accepted: 06 August 2026
Published: 13 August 2026

Research article

A regularized semi-discrete optimal control framework for recovering local volatility surfaces

Yun Liu[1,2], **Lifeng Guo**[1,2] **and Xijuan Liu**[1,2,*]

[1] College of Information Engineering, Tarim University, Alar, Xinjiang 843300, China
[2] Key Laboratory of Tarim Oasis Agriculture (Tarim University) Ministry of Education, Alar, Xinjiang 843300, China

* **Correspondence:** Email: lxjlychenchen@163.com.

Abstract: This paper uses standard time-stepping optimal control to construct a supplementary regularized method for recovering $\sigma(S,t)$ in the Black-Scholes model. With Dupire transformation, the volatility calibration problem becomes a coefficient identification problem of non-divergence parabolic equations. Combining Tikhonov regularization with a semi-discrete time stepping to break the two-dimensional inversion problem into a series of one-dimensional subproblems at each time layer, it reduces the inherent ill-posedness of the direct Dupire inversion. We derive forward-adjoint optimality conditions and uniform a priori bounds and prove that each discrete subproblem admits minimizers with existence, local uniqueness, and Lipschitz stability. Our main theoretical result shows that semi-discrete minimizers converge to the weak solution of the continuous regularized implied local volatility equation (RILVE) system when the time step approaches zero. Numerical simulations on synthetic flat, smile, and skew volatility data show that this layered regularized method can produce accurate volatility results and resist observational noise. This paper provides full theoretical deductions and numerical tests to support and improve the existing RILVE volatility inversion model.

Keywords: option pricing; implied volatility; parabolic coefficient inverse problem; optimal control; existence; Lipschitz stability
Mathematics Subject Classification: 35R30, 49J20, 91G20

1. Introduction

Since Black and Scholes [1] proposed the classical option pricing model, volatility has become a central concept in financial engineering and quantitative finance. The standard Black-Scholes model assumes constant volatility σ, which simplifies theoretical pricing but conflicts with real market data. In practice, option prices often exhibit two typical patterns: volatility smiles and volatility skews.

Volatility also varies with maturity, forming a term structure. These market facts prove volatility is not a fixed constant (see [2–5]). These observations indicate that real-world volatility possesses a complex dynamic structure–it is not constant but rather a bivariate function depending on both the underlying asset price S and time t, i.e., the local volatility surface $\sigma(S,t)$. Recovering this space-time volatility surface from market option prices is a key parabolic coefficient inverse problem in computational finance. The implied volatility inversion problem belongs mathematically to the class of coefficient identification problems for parabolic equations. Its core is to recover the diffusion coefficient (i.e., the volatility function) in the Black-Scholes equation from observed option prices. Dupire [6] derived an explicit relationship between option prices and local volatility and established the classic Dupire formula for direct computation. This work laid the foundation for calibrating local volatility model parameters. However, applying the Dupire formula directly to discrete market prices requires numerical differentiation, which is highly sensitive to noise and causes severe numerical instability the fundamental source of ill-posedness.

Many scholars designed regularization and optimal control methods to stabilize inversion and guarantee solution uniqueness (see [7–22]). Bouchouev and Isakov [12–14] transformed the problem into an inverse parabolic problem with terminal observation and established uniqueness and stability results. Jiang and Tao [15] explored the optimal control framework for the case volatility depending only on the underlying asset price $\sigma = \sigma(S)$. They proved the existence of an optimal solution and derived the corresponding optimality conditions, and the numerical simulations were later provided in [16]. Deng et al. [17] introduced "averaged option prices" as terminal conditions, extending the observation form of the inverse problem and enhancing the model's ability to extract information from market data.

Most papers only study time-independent volatility or purely theoretical analysis of space-time volatility (see [15–23]). Few complete frameworks can meet three demands at the same time: full theoretical support, strong noise resistance, and low computation cost. Jiang and Bian [18] proposed the regularized implied local volatility equation (RILVE), which provides a key approach for two-dimensional volatility surface inversion. This method, via time discretization and variational inequality coupling, constructs a fully nonlinear parabolic system that simultaneously recovers both $\sigma(S,t)$ and the option price and proves its stability and convergence. The determination of time-dependent volatility from observed market data was investigated in [19] by using a regularization technique with an entropy penalty.

However, two-dimensional volatility surface inversion still faces three core challenges: the curse of dimensionality leading to high computational complexity, time non-stationarity causing model adaptability issues, and the tendency of global optimization algorithms to converge to local minima. Inspired by Deng et al. [17], who successfully applied the time-stepping optimal control method to inverse heat conduction problems, we adapt this well-established semi-discrete framework into the financial RILVE inverse problem, which can be regarded as an effective extension of existing variational tools. We conjecture that the sequential decomposition strategy may alleviate full-grid computational burdens, though quantitative efficiency comparisons and complexity bounds are left for future study.

The RILVE provides a sound continuous model, but its numerical solution is challenging because the forward and adjoint equations are coupled. Solving both on a full grid yields large nonlinear systems that are expensive to compute. The time-stepping idea from [16] was designed for linear heat equations; transplanting it to the quasilinear Black-Scholes equation is not trivial. Earlier works [7, 8] studied similar inverse problems using variational regularization method but focused on the continuous problem or global grid schemes. Our work bridges the RILVE theory with practical computation by proposing a time-marching scheme and supplying a complete convergence proof. The existence, stability, and uniqueness results we establish are not merely new continuous theorems; they also serve as limit results that confirm the correctness of our numerical scheme.

Building on the RILVE framework proposed by Jiang and Bian [18], we transplant classical time-marching optimal control from parabolic inverse problems to decompose two-dimensional volatility inversion into sequential one-dimensional subproblems, offering supplementary theoretical and numerical extensions to the existing RILVE model: (i) We verify the well-posedness of each time-layer optimization subproblem, including existence, local uniqueness, and Lipschitz stability of minimizers. (ii) We derive coupled forward-adjoint optimality conditions and uniform a priori estimate and further prove semi-discrete minimizers converge to continuous RILVE weak solutions as the time step vanishes–this constitutes the core theoretical supplement of this work. (iii) We employ a standard finite-difference gradient descent to test three classic volatility profiles, providing extra numerical evidence for the reconstruction accuracy and noise robustness of regularized volatility calibration.

The paper is organized as follows: Section 2 formulates the problem and introduces the Dupire transformation. Section 3 constructs the regularized optimal control framework. Section 4 establishes a series of a priori estimates and auxiliary technical lemmas with complete proofs. Section 5 proves the existence of semi-discrete solutions and analyzes the continuous limit. The optimality conditions, stability, and uniqueness are discussed in Section 6. In Section 7 presents the numerical algorithm and experiments, demonstrating the effectiveness of the theoretical analysis and numerical scheme. Section 8 concludes the paper and suggests future research directions.

2. Problem formulation

Consider an asset price process S_t under the risk-neutral measure following the geometric Brownian motion

$$\frac{dS_t}{S_t} = (r - q)dt + \sigma(S_t, t)dW_t, \tag{2.1}$$

where r is the risk-free rate, $\sigma(S, t) > 0$ is the unknown local volatility function, q is the dividend yield, and W_t is a standard Brownian motion.

The price of a European call option $C(S, t; K, T)$ satisfies the Black-Scholes equation

$$\frac{\partial C}{\partial t} + \frac{1}{2}\sigma^2(S, t)S^2\frac{\partial^2 C}{\partial S^2} + (r - q)S\frac{\partial C}{\partial S} - rC = 0, \tag{2.2}$$

with the terminal condition given by the option's intrinsic value at maturity

$$C(S, T) = (S - K)^+, \tag{2.3}$$

where $(x)^+ = \max\{x, 0\}$, K is the strike price, and T is the maturity.

Let $v(K, T) = C(S_0, 0; K, T)$ denote the European call price at current time $t = 0$, with spot price S_0, strike K, and maturity T. By no-arbitrage arguments, v satisfies the Dupire equation [6]

$$\frac{\partial v}{\partial T} = \frac{1}{2}K^2\sigma^2(K,T)\frac{\partial^2 v}{\partial K^2} - (r-q)K\frac{\partial v}{\partial K} - qv, \tag{2.4}$$

with initial condition

$$v(K,0) = (S_0 - K)^+. \tag{2.5}$$

The Dupire equation directly links the volatility $\sigma(K,T)$ to partial derivatives of the option price. Its explicit solution can be expressed as

$$\sigma(K,T) = \sqrt{\frac{\frac{\partial v}{\partial T} + (r-q)K\frac{\partial v}{\partial K} + qv}{\frac{1}{2}K^2\frac{\partial^2 v}{\partial K^2}}}.$$

This formula reveals that volatility inversion is strongly dependent on the first and second partial derivatives of the option price, which is precisely the source of ill-posedness.

Inverse problem (IPOP): Given market-observed option prices $v^*(K,T)$ for all $K \in \mathbb{R}^+$, $T \in [T_1, T_2]$, find the volatility function $\sigma(K,T)$ such that

$$v(K,T;\sigma) = v^*(K,T). \tag{2.6}$$

This formulation constitutes a coefficient identification problem for a parabolic equation. Its ill-posed nature manifests in two aspects: high sensitivity to perturbations in the data v^* and potential non-uniqueness of the solution σ.

To simplify the domain and boundary treatment, we introduce the variable substitution (see [8, 15])

$$x = \ln\frac{K}{S_0}, \quad \tau = T, \quad u(x,\tau) = \frac{1}{S_0}e^{q\tau}v(S_0e^x,\tau), \quad a(x,\tau) = \frac{1}{2}\sigma^2(S_0e^x,\tau). \tag{2.7}$$

The Dupire equation (2.4) then transforms into the more compact parabolic form

$$u_\tau = a(x,\tau)(u_{xx} - u_x) - (r-q)u_x, \quad x \in \mathbb{R},\ \tau \in (0,\tau_2], \tag{2.8}$$

with initial condition

$$u(x,0) = u_0(x) := (1 - e^x)^+. \tag{2.9}$$

Equations (2.8)–(2.9) constitute the forward problem: Given the coefficient $a(x,\tau)$, solve for $u(x,\tau)$. The inverse problem is then becomes the following: **Recover the** $a(x,\tau)$ **from observed data** $u^*(x,\tau)$, where the volatility is recovered via $\sigma(S_0e^x,\tau) = \sqrt{2a(x,\tau)}$. This achieves a mathematical simplification of the volatility inversion problem.

Remark 2.1. *The initial data $u_0(x) = (1 - e^x)^+$ is nonzero only on $x \le 0$. For parabolic equations with uniformly bounded and positive diffusion coefficients $a(x,\tau) \in [\underline{a}, \bar{a}]$, the solution preserves exponential decay as $|x| \to \infty$: There exist constants $C, \alpha > 0$ depending only on $r, q, \underline{a}, \bar{a}$ such that*

$$|u(x,\tau)| + |u_x(x,\tau)| \le Ce^{-\alpha|x|}, \quad \forall x \in \mathbb{R},\ \tau \in [0,\tau_2].$$

This decay property eliminates infinite boundary terms in integration by parts. Hence, all integral operations in the remainder of this paper are valid without extra boundary corrections.

3. Optimal control framework

The core practical difficulty of two-dimensional space-time volatility inversion lies in the high-dimensional, severely ill-posed nature of the coefficient identification task. Drawing on sequential optimal control methods validated for heat conduction inverse problems [17], we apply this time-layer decomposition strategy to the RILVE inverse system.

Consider the observation time interval $[\tau_1, \tau_2]$, uniformly partitioned into N subintervals

$$\tau_1 = t_0 < t_1 < \cdots < t_N = \tau_2, \quad h = \frac{\tau_2 - \tau_1}{N}, \quad t_n = \tau_1 + nh. \tag{3.1}$$

At each time level t_n, we observe transformed market data

$$u_n^*(x) = u(x, t_n) + \varepsilon_n(x), \quad n = 1, 2, \cdots, N, \tag{3.2}$$

where $\varepsilon_n(x)$ denotes observation noise.

To ensure existence and satisfy financial constraints, we define the admissible control sets:

(1) Spatial admissible set (for each time-slice control variable)

$$\mathcal{A}_0 = \{a \in H^1(\mathbb{R}) \cap L^\infty(\mathbb{R}) \,\big|\, \underline{a} \le a(x) \le \bar{a}, \text{ a.e. } x \in \mathbb{R}\}.$$

(2) Full space-time admissible set (for continuous reconstruction)

$$\mathcal{A} = \Big\{a \in H^1(Q) \cap L^\infty([\tau_1, \tau_2]; H^1(\mathbb{R})) \,\big|\, \underline{a} \le a(x, \tau) \le \bar{a}, \text{ a.e. } (x, \tau) \in Q\Big\}, \tag{3.3}$$

where $Q = \mathbb{R} \times [\tau_1, \tau_2]$ and $0 < \underline{a} < \bar{a} < \infty$ are given positive constants representing the lower and upper bounds of the transformed volatility coefficient.

Remark 3.1. *The admissible control set $\mathcal{A}$ has the following important properties: $\underline{a} \le a \le \overline{a}$ excludes negative or infinite volatility, which is financially meaningful; $a \in H^1(Q)$ ensures sufficient smoothness of the coefficient for theoretical analysis.*

Following the standard sequential regularization design and the continuous RILVE model proposed by Jiang and Bian [18], we adopt the widely used layered Tikhonov cost functional for time-stepping inversion

$$J_n(a) = \frac{\delta}{2}\left(\frac{1}{h}\|a - a_{n-1}\|^2_{L^2(\mathbb{R})} + \|\nabla a\|^2_{L^2(\mathbb{R})}\right) + \frac{1}{2h}\|u(\cdot, t_n; a) - u^*(\cdot, t_n)\|^2_{L^2(\mathbb{R})}, \tag{3.4}$$

where $\delta > 0$ is the regularization parameter and $u(\cdot, t_n; a)$ is the solution of the state equation at time t_n. Physically, the first term enforces temporal smoothness of the volatility surface, the second term enforces spatial smoothness to suppress noise amplification, and the third term measures data fitting accuracy between model outputs and market observations.

Given an initial guess $a_0 \in \mathcal{A}_0$, we sequentially solve the following optimization problem sequence:

Problem (P_n): Given $a_0, a_1, \cdots, a_{n-1} \in \mathcal{A}_0$, find $a_n \in \mathcal{A}_0$ such that

$$J_n(a_n) = \min_{a \in \mathcal{A}_0} J_n(a). \tag{3.5}$$

At each time level, the corresponding state solution is constructed as follows. For a given $a \in \mathcal{A}_0$, define the piecewise linear interpolated coefficient

$$\hat{a}(x,\tau) = \begin{cases} \dfrac{\tau - t_{n-1}}{h} a(x) + \dfrac{t_n - \tau}{h} a_{n-1}(x), & t_{n-1} \le \tau \le t_n, \\ \dfrac{\tau - t_{k-1}}{h} a_k(x) + \dfrac{t_k - \tau}{h} a_{k-1}(x), & t_{k-1} \le \tau \le t_k,\ 1 \le k \le n-1. \end{cases} \tag{3.6}$$

The corresponding state solution $u(x,\tau;\hat{a})$ satisfies equations (2.8)–(2.9). By sequentially solving $P_1, \cdots, P_N$, we obtain the sequence $\{a_n\}_{n=0}^N$. Define the discrete reconstruction function

$$a^h(x,\tau) = \frac{\tau - t_{n-1}}{h} a_n(x) + \frac{t_n - \tau}{h} a_{n-1}(x), \quad \tau \in [t_{n-1}, t_n],\ n = 1, \cdots, N. \tag{3.7}$$

Remark 3.2. *The discrete reconstruction a^h is linear in time on each subinterval $[t_{n-1}, t_n]$; it satisfies $a^h(x, t_n) = a_n(x)$ at the nodes; and its time derivative is constant on each subinterval: $a^h_\tau = (a_n - a_{n-1})/h$.*

4. Uniform estimates

Before analyzing discrete minimizers and their limit behavior as $h \to 0$, we derive uniform a priori bounds independent of the time step h. The bounds in Lemmas 4.1–4.4 serve as technical prerequisites for convergence analysis, offering uniform boundedness, compactness, and Hölder continuity to extract convergent subsequences.

Lemma 4.1. *Let $a \in \mathcal{A}$ with $a_x \in L^\infty(Q)$, and let u be the solution of the state equation* (2.8)–(2.9). *Then there exists a constant $C > 0$ (depending only on $\underline{a}, \overline{a}, r, q, T$) such that*

$$\|u\|_{L^\infty(Q)} + \int_{\tau_1}^{\tau_2} \int_{\mathbb{R}} (|u_\tau|^2 + |u_{xx}|^2) dx d\tau + \sup_{\tau \in [\tau_1, \tau_2]} \int_{\mathbb{R}} |u_x|^2 dx \le C. \tag{4.1}$$

Proof. Multiply both sides of equation (2.8) by u and integrate over $\mathbb{R}$

$$\int_{\mathbb{R}} u u_\tau dx = \int_{\mathbb{R}} a u u_{xx} dx - \int_{\mathbb{R}} a u u_x dx - (r-q) \int_{\mathbb{R}} u u_x dx. \tag{4.2}$$

Since $u(x,\tau) \in H^1(\mathbb{R})$ and decays to 0 as $|x| \to \infty$ (by parabolic equation regularity [16]), all integrals converge absolutely. Compute term by term

$$\int_{\mathbb{R}} u u_\tau dx = \frac{1}{2} \frac{d}{d\tau} \|u\|_{L^2}^2, \tag{4.3}$$

$$\int_{\mathbb{R}} a u u_{xx} dx = -\int_{\mathbb{R}} (au)_x u_x dx = -\int_{\mathbb{R}} a_x u u_x dx - \int_{\mathbb{R}} a u_x^2 dx, \tag{4.4}$$

$$\int_{\mathbb{R}} a u u_x dx = \frac{1}{2} \int_{\mathbb{R}} a (u^2)_x dx = -\frac{1}{2} \int_{\mathbb{R}} a_x u^2 dx, \tag{4.5}$$

$$\int_{\mathbb{R}} u u_x dx = \frac{1}{2} \int_{\mathbb{R}} (u^2)_x dx = 0. \tag{4.6}$$

Substituting (4.3)–(4.6) back into (4.2) and simplifying yields the energy identity

$$\frac{1}{2}\frac{d}{d\tau}\|u\|_{L^2}^2 + \int_{\mathbb{R}} a u_x^2 dx = -\int_{\mathbb{R}} a_x u u_x dx + \frac{1}{2}\int_{\mathbb{R}} a_x u^2 dx. \tag{4.7}$$

Since $a_x \in L^\infty(Q)$, there exists a constant $M = \|a_x\|_{L^\infty(Q)} > 0$ such that $|a_x| \le M$ almost everywhere. Taking $\varepsilon = \frac{\underline{a}}{2}$ and applying Young's inequality [24], we obtain

$$\begin{aligned}\left|\int_{\mathbb{R}} a_x u u_x dx\right| &\le M \int_{\mathbb{R}} |u||u_x| dx \\ &\le \frac{\underline{a}}{4}\int_{\mathbb{R}} u_x^2 dx + \frac{M^2}{\underline{a}}\int_{\mathbb{R}} u^2 dx, \end{aligned} \tag{4.8}$$

$$\left|\frac{1}{2}\int_{\mathbb{R}} a_x u^2 dx\right| \le \frac{M}{2}\int_{\mathbb{R}} u^2 dx. \tag{4.9}$$

Substituting (4.8)–(4.9) into (4.7), then we have

$$\frac{d}{d\tau}\|u\|_{L^2}^2 + \frac{\underline{a}}{2}\int_{\mathbb{R}} u_x^2 dx \le \left(\frac{2M^2}{\underline{a}} + M\right)\|u\|_{L^2}^2. \tag{4.10}$$

Let $C_1 = \dfrac{2M^2}{\underline{a}} + M$, which depends only on $\underline{a}$ and the bound on a_x. By Gronwall's inequality, one can easily get

$$\|u(\tau)\|_{L^2}^2 \le \|u_0\|_{L^2}^2 e^{C_1(\tau-\tau_1)}, \quad \tau \in [\tau_1, \tau_2]. \tag{4.11}$$

Multiply both sides of equation (2.8) by $-u_{xx}$ and integrate over $\mathbb{R}$

$$-\int_{\mathbb{R}} u_\tau u_{xx} dx = -\int_{\mathbb{R}} a u_{xx}^2 dx + \int_{\mathbb{R}} a u_x u_{xx} dx + (r-q)\int_{\mathbb{R}} u_x u_{xx} dx. \tag{4.12}$$

The left-hand side becomes

$$-\int_{\mathbb{R}} u_\tau u_{xx} dx = \int_{\mathbb{R}} u_{\tau x} u_x dx = \frac{1}{2}\frac{d}{d\tau}\|u_x\|_{L^2}^2. \tag{4.13}$$

Bound each term on the right-hand side using Young's inequality

$$\begin{aligned}\left|\int_{\mathbb{R}} a u_x u_{xx} dx\right| &\le \overline{a}\int_{\mathbb{R}} |u_x||u_{xx}| dx \\ &\le \frac{\underline{a}}{4}\int_{\mathbb{R}} u_{xx}^2 dx + \frac{\overline{a}^2}{\underline{a}}\int_{\mathbb{R}} u_x^2 dx, \end{aligned} \tag{4.14}$$

$$\left|(r-q)\int_{\mathbb{R}} u_x u_{xx} dx\right| \le |r-q|\left(\frac{\underline{a}}{4}\int_{\mathbb{R}} u_{xx}^2 dx + \frac{1}{\underline{a}}\int_{\mathbb{R}} u_x^2 dx\right). \tag{4.15}$$

Substituting (4.13)–(4.15) into (4.12) yields

$$\frac{1}{2}\frac{d}{d\tau}\|u_x\|_{L^2}^2 + \frac{\underline{a}}{4}\int_{\mathbb{R}} u_{xx}^2 dx \le C_2\int_{\mathbb{R}} u_x^2 dx, \tag{4.16}$$

where $C_2 = \frac{\overline{a}^2+(r-q)^2}{\underline{a}}$, depending only on volatility bounds and market parameters.

Adding (4.10) and (4.16), we can obtain

$$\frac{d}{d\tau}(\|u\|_{L^2}^2 + \|u_x\|_{L^2}^2) + \frac{\underline{a}}{4}(\|u_x\|_{L^2}^2 + \|u_{xx}\|_{L^2}^2) \le C_3(\|u\|_{L^2}^2 + \|u_x\|_{L^2}^2), \tag{4.17}$$

where $C_3 = \max\{C_1, C_2\}$. Applying Gronwall's inequality again

$$\|u(\tau)\|_{H^1}^2 \le \|u_0\|_{H^1}^2 e^{C_3(\tau-\tau_1)}. \tag{4.18}$$

To estimate u_τ, let $v = u_\tau$ and differentiate the state equation with respect to τ

$$v_\tau = a(v_{xx} - v_x) + a_\tau(u_{xx} - u_x) - (r-q)v_x. \tag{4.19}$$

This is a linear parabolic equation for v with forcing term $f = a_\tau(u_{xx} - u_x)$. Since $u_{xx}, u_x \in L^2(Q)$, from the definition of $\mathcal{A}$, we have $a_\tau \in L^2(0,\tau_2; L^\infty(\mathbb{R}))$, hence $f \in L^2(Q)$. Applying the same energy inequality and the Gronwall argument to (4.19), with initial condition $v(\cdot,\tau_1)$ determined by substituting the initial data into the original state equation, yields

$$\sup_{\tau\in[\tau_1,\tau_2]} \|v(\cdot,\tau)\|_{L^2}^2 + \int_{\tau_1}^{\tau_2} \|v_x(\cdot,\tau)\|_{L^2}^2\, d\tau \le C\left(\|v(\cdot,\tau_1)\|_{L^2}^2 + \|f\|_{L^2(Q)}^2\right).$$

Combining with the earlier bounds for u_{xx} and u_x, we obtain

$$\int_{\tau_1}^{\tau_2}\int_{\mathbb{R}} \left(|u_x|^2 + |u_{xx}|^2\right) dx\, d\tau \le C. \tag{4.20}$$

The L^∞ bound for u follows from the Sobolev embedding $H^1(\mathbb{R}) \hookrightarrow L^\infty(\mathbb{R})$ combined with the uniform H^1 bound. Combining (4.11), (4.18), and (4.20) gives estimate (4.1). □

The adjoint equation plays a key role in deriving optimality conditions and handling data fitting terms. We next establish complete uniform regularity estimates for adjoint solutions.

Lemma 4.2. *Let ϕ satisfy the adjoint equation*

$$-\phi_\tau - (a\phi)_{xx} + (a\phi)_x - (r-q)\phi_x = 0, \quad (x,\tau) \in Q, \tag{4.21}$$

$$\phi(x,\tau_2) = u(x,\tau_2) - u^*(x,\tau_2), \quad x \in \mathbb{R}. \tag{4.22}$$

There exists a constant $C = C(r,q,\underline{a},\bar{a}) > 0$ such that

$$\|\phi\|_{L^\infty(Q)} + \int_{\tau_1}^{\tau_2}\int_{\mathbb{R}} (|\phi_\tau|^2 + |\phi_{xx}|^2) dx d\tau \le C\|u - u^*\|_{L^\infty(L^2)}. \tag{4.23}$$

Proof. We transform the adjoint equation into standard form via variable change and then perform energy estimates. Let $\psi = a\phi$ and compute derivatives

$$\psi_x = a_x\phi + a\phi_x, \tag{4.24}$$

$$\psi_{xx} = a_{xx}\phi + 2a_x\phi_x + a\phi_{xx}. \tag{4.25}$$

Substituting $\phi = \psi/a$ into equation (4.21) and performing detailed calculations yields

$$\psi_\tau + a\psi_{xx} + b\psi_x + c\psi = 0, \tag{4.26}$$

where the coefficients are

$$b = 2a_x - 1 + (r - q), \tag{4.27}$$
$$c = a_{xx} - a_x. \tag{4.28}$$

Since $a \in \mathcal{A}$, there exists a constant C such that $\|b\|_{L^\infty}, \|c\|_{L^\infty} \leq C$.
Multiply equation (4.26) by ψ and integrate over $\mathbb{R}$

$$\int_{\mathbb{R}} \psi\psi_\tau dx + \int_{\mathbb{R}} a\psi\psi_{xx} dx + \int_{\mathbb{R}} b\psi\psi_x dx + \int_{\mathbb{R}} c\psi^2 dx = 0. \tag{4.29}$$

Computing term by term

$$\int_{\mathbb{R}} \psi\psi_\tau dx = \frac{1}{2}\frac{d}{d\tau}\|\psi\|_{L^2}^2, \tag{4.30}$$
$$\int_{\mathbb{R}} a\psi\psi_{xx} dx = -\int_{\mathbb{R}} (a\psi)_x\psi_x dx = -\int_{\mathbb{R}} a_x\psi\psi_x dx - \int_{\mathbb{R}} a\psi_x^2 dx. \tag{4.31}$$

Substituting into (4.29) gives

$$\frac{1}{2}\frac{d}{d\tau}\|\psi\|_{L^2}^2 + \int_{\mathbb{R}} a\psi_x^2 dx = -\int_{\mathbb{R}} b\psi\psi_x dx - \int_{\mathbb{R}} c\psi^2 dx + \int_{\mathbb{R}} a_x\psi\psi_x dx. \tag{4.32}$$

Apply Young's inequality to estimate the right-hand side

$$\left|\int_{\mathbb{R}} b\psi\psi_x dx\right| \leq \|b\|_{L^\infty}\left(\frac{\underline{a}}{4}\int_{\mathbb{R}} \psi_x^2 dx + \frac{1}{\underline{a}}\int_{\mathbb{R}} \psi^2 dx\right), \tag{4.33}$$
$$\left|\int_{\mathbb{R}} c\psi^2 dx\right| \leq \|c\|_{L^\infty}\int_{\mathbb{R}} \psi^2 dx, \tag{4.34}$$
$$\left|\int_{\mathbb{R}} a_x\psi\psi_x dx\right| \leq M\left(\frac{\underline{a}}{4}\int_{\mathbb{R}} \psi_x^2 dx + \frac{1}{\underline{a}}\int_{\mathbb{R}} \psi^2 dx\right). \tag{4.35}$$

Substituting into (4.32) and rearranging yields

$$\frac{d}{d\tau}\|\psi\|_{L^2}^2 + \frac{\underline{a}}{2}\|\psi_x\|_{L^2}^2 \leq C\|\psi\|_{L^2}^2. \tag{4.36}$$

Introduce reverse time $s = \tau_2 - \tau$. Then equation (4.26) becomes

$$\psi_s - a\psi_{xx} - b\psi_x - c\psi = 0. \tag{4.37}$$

By the maximum principle for parabolic equations

$$\sup_Q |\psi| \leq \sup_{\mathbb{R}} |\psi(\cdot, 0)| = \sup_{\mathbb{R}} |a(\cdot, \tau_2)[u(\cdot, \tau_2) - u^*(\cdot, \tau_2)]|. \tag{4.38}$$

Since $a \leq \overline{a}$, we have

$$\|\psi\|_{L^\infty(Q)} \leq \overline{a}\|u(\cdot,\tau_2) - u^*(\cdot,\tau_2)\|_{L^\infty}. \tag{4.39}$$

Since $\phi = \psi/a$ and $a \geq \underline{a} > 0$, we obtain

$$\|\phi\|_{L^\infty(Q)} \leq \frac{\overline{a}}{\underline{a}}\|u(\cdot,\tau_2) - u^*(\cdot,\tau_2)\|_{L^\infty}. \tag{4.40}$$

Performing higher-order energy estimates on equation (4.26) similar to Lemma 4.1 yields

$$\int_{\tau_1}^{\tau_2}\int_{\mathbb{R}}(|\psi_\tau|^2 + |\psi_{xx}|^2)dxd\tau \leq C\|\psi\|_{L^\infty(Q)}. \tag{4.41}$$

Since $\phi = \psi/a$ and a is uniformly positive and smooth, the corresponding bounds for ϕ_τ and ϕ_{xx} follow directly by the product rule for derivatives. Combining all estimates yields the target inequality (4.23). □

Uniform boundedness for semi-discrete reconstructions is essential to analyze the continuous limit as $h \to 0$. The following bounds hold uniformly with respect to time step h.

Lemma 4.3. *Let a_n be the optimal solution of problem (P_n), and let a^h be its linear interpolation function* (3.7)*. Then there exists a constant $C > 0$ independent of h such that:*

$$\sum_{n=1}^{N}\frac{\|a_n - a_{n-1}\|^2_{L^2(\mathbb{R})}}{h} + \max_{1\leq n\leq N}\|\nabla a_n\|^2_{L^2(\mathbb{R})} \leq C, \tag{4.42}$$

$$\int_{\tau_1}^{\tau_2}\|a^h_\tau\|^2_{L^2(\mathbb{R})}d\tau + \sup_{\tau\in[\tau_1,\tau_2]}\|\nabla a^h(\cdot,\tau)\|^2_{L^2(\mathbb{R})} \leq C. \tag{4.43}$$

Proof. Since a_n is the optimal solution of (P_n), taking $a = a_{n-1}$ for comparison gives

$$J_n(a_n) \leq J_n(a_{n-1}). \tag{4.44}$$

Expanding the cost functional (3.4)

$$\begin{aligned}\frac{\delta}{2h}\|a_n - a_{n-1}\|^2_{L^2} + \frac{\delta}{2}\|\nabla a_n\|^2_{L^2} + \frac{1}{2h}\|u_n - u_n^*\|^2_{L^2}&\\ \leq \frac{\delta}{2}\|\nabla a_{n-1}\|^2_{L^2} + \frac{1}{2h}\|u_{n-1} - u_n^*\|^2_{L^2},&\end{aligned} \tag{4.45}$$

where $u_n = u(\cdot, t_n; a_n)$ and $u_{n-1} = u(\cdot, t_n; a_{n-1})$.

Rearranging gives the basic inequality

$$\frac{\delta}{2h}\|a_n - a_{n-1}\|^2_{L^2} + \frac{\delta}{2}(\|\nabla a_n\|^2_{L^2} - \|\nabla a_{n-1}\|^2_{L^2}) \leq \frac{1}{2h}(\|u_{n-1} - u_n^*\|^2_{L^2} - \|u_n - u_n^*\|^2_{L^2}). \tag{4.46}$$

To estimate the right-hand side, let $w = u_{n-1} - u_n$. Then w satisfies

$$w_\tau = a_{n-1}(w_{xx} - w_x) - (r - q)w_x + (a_{n-1} - a_n)(u_{n,xx} - u_{n,x}), \tag{4.47}$$

$$w(\cdot, t_{n-1}) = 0. \tag{4.48}$$

Multiply equation (4.47) by w and integrate over $\mathbb{R} \times [t_{n-1}, \tau]$, which gives

$$\frac{1}{2}\|w(\tau)\|_{L^2}^2 + \int_{t_{n-1}}^{\tau} \int_{\mathbb{R}} a_{n-1} w_x^2 dxds = I_1 + I_2, \tag{4.49}$$

where

$$I_1 = \int_{t_{n-1}}^{\tau} \int_{\mathbb{R}} (a_{n-1} - a_n)(u_{n,xx} - u_{n,x}) w dxds, \tag{4.50}$$

$$I_2 = \int_{t_{n-1}}^{\tau} \int_{\mathbb{R}} [a_{n-1} w w_x - (r-q) w w_x] dxds. \tag{4.51}$$

Estimate I_1: By the Cauchy-Schwarz inequality [24] and Lemma 4.1, then we have

$$|I_1| \le \|a_n - a_{n-1}\|_{L^2} \cdot \|u_{n,xx} - u_{n,x}\|_{L^2} \cdot \|w\|_{L^2} \le C\|a_n - a_{n-1}\|_{L^2} \cdot \|w\|_{L^2}. \tag{4.52}$$

Estimate I_2: Applying Young's inequality,

$$|I_2| \le \frac{\underline{a}}{4} \int_{t_{n-1}}^{\tau} \|w_x\|_{L^2}^2 ds + C \int_{t_{n-1}}^{\tau} \|w\|_{L^2}^2 ds. \tag{4.53}$$

Substituting into (4.49) yields

$$\frac{1}{2}\|w(\tau)\|_{L^2}^2 + \frac{3\underline{a}}{4} \int_{t_{n-1}}^{\tau} \|w_x\|_{L^2}^2 ds \le C \int_{t_{n-1}}^{\tau} \|w\|_{L^2}^2 ds + C\|a_n - a_{n-1}\|_{L^2} \|w\|_{L^2}. \tag{4.54}$$

Applying Gronwall's inequality

$$\|w(\tau)\|_{L^2}^2 \le C\|a_n - a_{n-1}\|_{L^2}^2 \int_{t_{n-1}}^{\tau} e^{C(\tau - s)} ds \le Ch\|a_n - a_{n-1}\|_{L^2}^2. \tag{4.55}$$

In particular, at $\tau = t_n$

$$\|u_{n-1} - u_n\|_{L^2} \le C\sqrt{h}\|a_n - a_{n-1}\|_{L^2}. \tag{4.56}$$

Next, estimate the right-hand side of (4.46)

$$\begin{aligned} &\|u_{n-1} - u_n^*\|_{L^2}^2 - \|u_n - u_n^*\|_{L^2}^2 \\ &\qquad = \|u_{n-1} - u_n + u_n - u_n^*\|_{L^2}^2 - \|u_n - u_n^*\|_{L^2}^2 \\ &\qquad = \|u_{n-1} - u_n\|_{L^2}^2 + 2\langle u_{n-1} - u_n, u_n - u_n^* \rangle. \end{aligned} \tag{4.57}$$

By (4.56) and the Cauchy-Schwarz inequality

$$\left|\langle u_{n-1} - u_n, u_n - u_n^* \rangle\right| \le \|u_{n-1} - u_n\|_{L^2} \cdot \|u_n - u_n^*\|_{L^2} \le C\sqrt{h}\|a_n - a_{n-1}\|_{L^2}. \tag{4.58}$$

Combining with (4.55) gives

$$\|u_{n-1} - u_n^*\|_{L^2}^2 - \|u_n - u_n^*\|_{L^2}^2 \le Ch\|a_n - a_{n-1}\|_{L^2}^2 + C\sqrt{h}\|a_n - a_{n-1}\|_{L^2}. \tag{4.59}$$

Substitute (4.59) into the basic inequality (4.46)

$$\frac{\delta}{2h}\|a_n - a_{n-1}\|_{L^2}^2 + \frac{\delta}{2}(\|\nabla a_n\|_{L^2}^2 - \|\nabla a_{n-1}\|_{L^2}^2) \le \frac{C}{h}\left(h\|a_n - a_{n-1}\|_{L^2}^2 + \sqrt{h}\|a_n - a_{n-1}\|_{L^2}\right). \tag{4.60}$$

Rearranging terms gives

$$\frac{\delta}{2h}\|a_n - a_{n-1}\|_{L^2}^2 + \frac{\delta}{2}(\|\nabla a_n\|_{L^2}^2 - \|\nabla a_{n-1}\|_{L^2}^2) \le C\|a_n - a_{n-1}\|_{L^2}^2 + \frac{C}{\sqrt{h}}\|a_n - a_{n-1}\|_{L^2}. \tag{4.61}$$

Apply Young's inequality to the last term

$$\frac{C}{\sqrt{h}}\|a_n - a_{n-1}\|_{L^2} \le \frac{\delta}{4h}\|a_n - a_{n-1}\|_{L^2}^2 + \frac{C^2 h}{\delta}. \tag{4.62}$$

Substituting into (4.61) gives

$$\frac{\delta}{4h}\|a_n - a_{n-1}\|_{L^2}^2 + \frac{\delta}{2}(\|\nabla a_n\|_{L^2}^2 - \|\nabla a_{n-1}\|_{L^2}^2) \le C\|a_n - a_{n-1}\|_{L^2}^2 + \frac{C^2 h}{\delta}. \tag{4.63}$$

For sufficiently small h, we have $C\|a_n - a_{n-1}\|_{L^2}^2 \le \frac{\delta}{8h}\|a_n - a_{n-1}\|_{L^2}^2$, hence

$$\frac{\delta}{8h}\|a_n - a_{n-1}\|_{L^2}^2 + \frac{\delta}{2}(\|\nabla a_n\|_{L^2}^2 - \|\nabla a_{n-1}\|_{L^2}^2) \le \frac{C^2 h}{\delta}. \tag{4.64}$$

Summing (4.64) from $n = 1, \cdots, k$, then we have

$$\frac{\delta}{8}\sum_{n=1}^{k}\frac{\|a_n - a_{n-1}\|_{L^2}^2}{h} + \frac{\delta}{2}\|\nabla a_k\|_{L^2}^2 \le \frac{\delta}{2}\|\nabla a_0\|_{L^2}^2 + \frac{C^2 kh}{\delta}. \tag{4.65}$$

Since $kh \le \tau_2 - \tau_1$, we obtain

$$\sum_{n=1}^{N}\frac{\|a_n - a_{n-1}\|_{L^2}^2}{h} + \max_{1\le n\le N}\|\nabla a_n\|_{L^2}^2 \le C. \tag{4.66}$$

By the interpolation definition (3.7), $a_\tau^h = (a_n - a_{n-1})/h$, thus

$$\int_{\tau_1}^{\tau_2}\|a_\tau^h\|_{L^2}^2 d\tau = \sum_{n=1}^{N} h \cdot \frac{\|a_n - a_{n-1}\|_{L^2}^2}{h^2} = \sum_{n=1}^{N}\frac{\|a_n - a_{n-1}\|_{L^2}^2}{h} \le C. \tag{4.67}$$

Meanwhile, $\|\nabla a^h(\cdot,\tau)\|_{L^2}^2$ is controlled by linear interpolation and does not exceed $\max_n \|\nabla a_n\|_{L^2}^2$, hence (4.43) holds. □

Lemma 4.4. *For the discrete reconstruction a^h, the following Hölder estimate holds*

$$\|a^h\|_{C^{1/2,1/4}(\bar{Q})} \le C\left(\|\nabla a^h\|_{L^2(Q)} + \|a_\tau^h\|_{L^2(Q)}\right). \tag{4.68}$$

Proof. The proof consists of Hölder estimates in space and time directions. By the Sobolev embedding theorem ($H^1(\mathbb{R}) \hookrightarrow C^{1/2}(\mathbb{R})$), for fixed time τ

$$|a^h(x,\tau) - a^h(y,\tau)| \le C\|a^h(\cdot,\tau)\|_{H^1}|x-y|^{1/2}, \tag{4.69}$$

where $\|a^h(\cdot,\tau)\|_{H^1}^2 = \|a^h(\cdot,\tau)\|_{L^2}^2 + \|\nabla a^h(\cdot,\tau)\|_{L^2}^2$.

By Lemma 4.3, $\sup_\tau \|\nabla a^h(\cdot,\tau)\|_{L^2} \le C$, and $\|a^h\|_{L^\infty} \le \overline{a}$, hence

$$|a^h(x,\tau) - a^h(y,\tau)| \le C|x-y|^{1/2}. \tag{4.70}$$

For fixed x, consider $\tau, s \in [\tau_1, \tau_2]$ with $s < \tau$. By definition

$$a^h(x,\tau) - a^h(x,s) = \int_s^\tau a^h_\tau(x,r)dr. \tag{4.71}$$

Thus

$$\begin{aligned} |a^h(x,\tau) - a^h(x,s)| &\le \int_s^\tau |a^h_\tau(x,r)|dr \\ &\le \left(\int_s^\tau |a^h_\tau(x,r)|^2 dr\right)^{1/2} |\tau - s|^{1/2}. \end{aligned} \tag{4.72}$$

Integrating over x gives the L^2 norm estimate

$$\|a^h(\cdot,\tau) - a^h(\cdot,s)\|_{L^2} \le \|a^h_\tau\|_{L^2(Q)}|\tau - s|^{1/2}. \tag{4.73}$$

For any interval $I \subset \mathbb{R}$, by the Sobolev embedding $H^1(I) \hookrightarrow C^{1/2}(I)$

$$\sup_{x\in I} |a^h(x,\tau) - a^h(x,s)| \le C\|a^h(\cdot,\tau) - a^h(\cdot,s)\|_{H^1(I)}. \tag{4.74}$$

Compute the H^1 norm

$$\begin{aligned} \|a^h(\cdot,\tau) - a^h(\cdot,s)\|_{H^1(I)} &\le \|a^h(\cdot,\tau) - a^h(\cdot,s)\|_{L^2(I)} + \|\nabla a^h(\cdot,\tau) - \nabla a^h(\cdot,s)\|_{L^2(I)} \\ &=: T_1 + T_2. \end{aligned} \tag{4.75}$$

T_1 is controlled by (4.73). For T_2, interchange the gradient and time integration

$$\nabla a^h(x,\tau) - \nabla a^h(x,s) = \int_s^\tau \nabla a^h_\tau(x,r)dr. \tag{4.76}$$

Apply the Cauchy-Schwarz inequality again

$$\begin{aligned} T_2 &= \|\nabla a^h(\cdot,\tau) - \nabla a^h(\cdot,s)\|_{L^2(I)} \\ &\le \int_s^\tau \|\nabla a^h_\tau(\cdot,r)\|_{L^2(I)}dr \\ &\le |\tau - s|^{1/2}\left(\int_s^\tau \|\nabla a^h_\tau(\cdot,r)\|^2_{L^2(I)}dr\right)^{1/2}. \end{aligned} \tag{4.77}$$

Combining the spatial Hölder estimate (4.70) and (4.73), and applying the interpolation inequality for Hölder spaces (see [24, 25]), we obtain the desired joint Hölder estimate in space and time (4.68). □

5. Existence, convergence, and optimality of semi-discrete optimal control

This section contains two core theoretical analyses. First, using the direct variational method with minimizing sequences and compactness theory, we prove the existence of an optimal solution to each semi-discrete problem (P_n). Second, we study the asymptotic behavior of discrete sequence $\{a^h\}$ for $h \to 0$. Compactness arguments extract convergent subsequences whose limits satisfy a coupled parabolic system, and we derive the associated first-order optimality conditions. These results connect discrete numerical approximations to the continuous regularized volatility model.

Theorem 5.1. *Suppose the following conditions hold:*

(1) Observed data $u^* \in C^{\alpha,\alpha/2}(\bar{Q})$ for some $\alpha \in (0,1)$, with $\|u^*\|_{C^{\alpha,\alpha/2}(\bar{Q})} \leq C$, where C is a positive constant independent of u^*;

(2) Initial data $u_0 \in H^1(\mathbb{R})$, initial control guess $a_0 \in \mathcal{A}_0$;

(3) Model parameters $r, q \in \mathbb{R}$, and time interval length $T = \tau_2 - \tau_1 > 0$, with time step $h = \frac{T}{N}$, where $N \in \mathbb{N}^+$ is the number of discrete time steps.

Then for each $n = 1, 2, \cdots, N$, the semi-discrete optimization problem (P_n) admits at least one optimal solution $a_n \in \mathcal{A}_0$.

Proof. The admissible set $\mathcal{A}_0$ defined above is a closed and convex subset of $H^1(Q)$, hence it is also weakly closed. We prove the existence by verifying coercivity and weak lower semi-continuity of the cost functional $J_n(a)$ on $\mathcal{A}_0$.

For $a \in \mathcal{A}_0$, the cost functional is

$$J_n(a) = \frac{1}{2h}\|u(\cdot, t_n; a) - u_n^*\|_{L^2}^2 + \frac{\delta}{2}\|\nabla a\|_{L^2}^2.$$

By Lemma 4.1, $\|u(\cdot, t_n; a)\|_{L^2} \leq C$ (independent of a), so the data fitting term satisfies

$$\frac{1}{2h}\|u - u_n^*\|_{L^2}^2 \geq \frac{1}{2h}\left(\|u_n^*\|_{L^2} - \|u\|_{L^2}\right)^2 \geq -\frac{C}{h}\|u_n^*\|_{L^2} + \frac{1}{2h}\|u_n^*\|_{L^2}^2 \geq -C',$$

where C' is a constant independent of a. Thus

$$J_n(a) \geq \frac{\delta}{2}\|\nabla a\|_{L^2}^2 - C',$$

when $\|\nabla a\|_{L^2} \to \infty$, $J_n(a) \to \infty$, which proves coercivity.

Since J_n is non-negative and bounded below on $\mathcal{A}$

$$m = \inf_{a \in \mathcal{A}} J_n(a) \geq 0. \tag{5.1}$$

Take a minimizing sequence $\{a^{(k)}\} \subset \mathcal{A}$, such that

$$\lim_{k \to \infty} J_n(a^{(k)}) = m. \tag{5.2}$$

By coercivity, $\{a^{(k)}\}$ is bounded in H^1, i.e., there exists a constant M, such that

$$\|a^{(k)}\|_{H^1} \leq M. \tag{5.3}$$

By the reflexivity of H^1 and weak closedness of $\mathcal{A}$, there exists a subsequence (still denoted $\{a^{(k)}\}$) and $a_n \in \mathcal{A}$, such that

$$a^{(k)} \rightharpoonup a_n \quad \text{weakly in } H^1. \tag{5.4}$$

By the Sobolev compact embedding theorem, we further have

$$a^{(k)} \to a_n \quad \text{strongly in } L^2. \tag{5.5}$$

The regularization term $\|\nabla a\|_{L^2}^2$ is weakly lower semi-continuous on $H^1(\mathbb{R})$. We additionally prove continuity of the state-to-control map: When a control sequence converges weakly in H^1, the corresponding state solutions converge strongly in L^2; hence the data misfit term (a continuous functional of the state) is also weakly lower semi-continuous. Therefore the full cost functional J_n is weakly lower semi-continuous

$$\liminf_{k\to\infty} J_n(a^{(k)}) \geq J_n(a_n). \tag{5.6}$$

On the other hand, since $\{a^{(k)}\}$ is a minimizing sequence

$$\lim_{k\to\infty} J_n(a^{(k)}) = m. \tag{5.7}$$

Therefore

$$m \geq J_n(a_n). \tag{5.8}$$

By the definition of m: $m = \inf_{a\in\mathcal{A}} J_n(a) \leq J_n(a_n)$, we must have $J_n(a_n) = m$, i.e., a_n attains the minimum. Consequently, a_n is an optimal solution of problem (P_n). □

Theorem 5.2. *Let a_n be the optimal solution to the problem (P_n), then for any $w \in \mathcal{A}$, the following variational inequality holds*

$$\int_{\mathbb{R}} \left[\frac{a_n - a_{n-1}}{h}(w - a_n) + \nabla a_n \cdot \nabla(w - a_n) + f_n(w - a_n) \right] dx \geq 0, \tag{5.9}$$

where

$$f_n(x) = \frac{1}{\delta h} \int_{t_{n-1}}^{t_n} \frac{\tau - t_{n-1}}{h} \phi^h(x,\tau) u_{xx}^h(x,\tau) d\tau. \tag{5.10}$$

ϕ^h is the adjoint variable satisfying

$$-\phi_\tau^h - (a^h\phi^h)_{xx} + (a^h\phi^h)_x - (r-q)\phi_x^h + q\phi^h = 0, \tag{5.11}$$

$$\phi^h(x,t_n) = u^h(x,t_n) - u^*(x,t_n). \tag{5.12}$$

Proof. For convex admissible set $\mathcal{A}_0$, for any $\lambda \in [0,1]$, the convex combination is

$$a^\lambda = (1-\lambda)a_n + \lambda w \in \mathcal{A}_0. \tag{5.13}$$

Consider the function $g(\lambda) = J_n(a^\lambda)$. Since a_n is a minimizer, $g(\lambda)$ attains its minimum at $\lambda = 0$, hence $g'(0) \geq 0$. Direct computation of $g'(\lambda)$ gives

$$g'(\lambda) = \frac{\delta}{h} \int_{\mathbb{R}} (a^\lambda - a_{n-1})(w - a_n) dx + \delta \int_{\mathbb{R}} \nabla a^\lambda \cdot \nabla(w - a_n) dx$$

$$+\frac{1}{h}\int_{\mathbb{R}}(u^{\lambda}(x,t_n)-u_n^*(x))\frac{du^{\lambda}(x,t_n)}{d\lambda}dx. \tag{5.14}$$

where $u^{\lambda}=u(\cdot,t_n;a^{\lambda})$.

Let $\xi^{\lambda}=\frac{du^{\lambda}}{d\lambda}$, Differentiating the state equation with respect to λ yields that ξ^{λ} satisfies

$$\xi^{\lambda}_{\tau}=a^{\lambda}(\xi^{\lambda}_{xx}-\xi^{\lambda}_{x})-(r-q)\xi^{\lambda}_{x}+(w-a_n)(u^{\lambda}_{xx}-u^{\lambda}_{x}), \tag{5.15}$$
$$\xi^{\lambda}(x,t_{n-1})=0. \tag{5.16}$$

Let ϕ^{λ} satisfy the adjoint equation

$$-\phi^{\lambda}_{\tau}-(a^{\lambda}\phi^{\lambda})_{xx}+(a^{\lambda}\phi^{\lambda})_{x}-(r-q)\phi^{\lambda}_{x}+q\phi^{\lambda}=0, \tag{5.17}$$
$$\phi^{\lambda}(x,t_n)=u^{\lambda}(x,t_n)-u_n^*(x). \tag{5.18}$$

Apply Green's formula to ϕ^{λ} and ξ^{λ}

$$\begin{aligned}0&=\int_{t_{n-1}}^{t_n}\int_{\mathbb{R}}\xi^{\lambda}\left[-\phi^{\lambda}_{\tau}-(a^{\lambda}\phi^{\lambda})_{xx}+(a^{\lambda}\phi^{\lambda})_{x}-(r-q)\phi^{\lambda}_{x}+q\phi^{\lambda}\right]dxd\tau\\&=-\int_{\mathbb{R}}\xi^{\lambda}(x,t_n)\phi^{\lambda}(x,t_n)dx+\int_{t_{n-1}}^{t_n}\int_{\mathbb{R}}\phi^{\lambda}\left[\xi^{\lambda}_{\tau}-(a^{\lambda}\xi^{\lambda})_{xx}+(a^{\lambda}\xi^{\lambda})_{x}-(r-q)\xi^{\lambda}_{x}+q\xi^{\lambda}\right]dxd\tau.\end{aligned}$$

Substituting (5.15) and (5.18) gives

$$\int_{\mathbb{R}}(u^{\lambda}(x,t_n)-u_n^*(x))\frac{du^{\lambda}(x,t_n)}{d\lambda}dx=\int_{t_{n-1}}^{t_n}\int_{\mathbb{R}}\phi^{\lambda}(w-a_n)(u^{\lambda}_{xx}-u^{\lambda}_{x})dxd\tau. \tag{5.19}$$

Setting $\lambda=0$ in (5.19) (note that $a^0=a_n$, $u^0=u_n$, $\phi^0=\phi$) yields

$$\int_{\mathbb{R}}(u_n-u_n^*)\frac{du^{\lambda}}{d\lambda}\bigg|_{\lambda=0}dx=\int_{t_{n-1}}^{t_n}\int_{\mathbb{R}}\phi(w-a_n)(u_{n,xx}-u_{n,x})dxd\tau. \tag{5.20}$$

Substituting into (5.14) with $\lambda=0$

$$\begin{aligned}g'(0)=&\frac{\delta}{h}\int_{\mathbb{R}}(a_n-a_{n-1})(w-a_n)dx+\delta\int_{\mathbb{R}}\nabla a_n\cdot\nabla(w-a_n)dx\\&+\frac{1}{h}\int_{t_{n-1}}^{t_n}\int_{\mathbb{R}}\phi(w-a_n)(u_{n,xx}-u_{n,x})dxd\tau\geq 0.\end{aligned} \tag{5.21}$$

Noting that on $[t_{n-1},t_n]$, a^h is linear, and ϕ^h , u^h correspond to discrete reconstructions, thus we obtain (5.9) after rearrangement. □

The theorem below establishes the compactness and convergence properties of semi-discrete volatility reconstruction sequences. It proves that as the time step $h\to 0$, the discrete minimizers obtained via layer-wise optimization converge uniformly to the solution of the continuous RILVE system, which verifies the self-consistency of the semi-discrete time-stepping regularization framework proposed in this paper.

Theorem 5.3. *There exists a subsequence of time steps $\{h_m\}$ with $h_m \to 0$ as $m \to 0$, and a limit volatility coefficient $a \in \mathcal{A}$, such that*

$$a^{h_m} \to a \quad \textit{uniformly in } C^{\frac{1}{2},\frac{1}{4}}(\bar{Q}), \tag{5.22}$$

where $\bar{Q} = \mathbb{R}[\tau_1, \tau_1]$ denotes the closure of the spatio-temporal domain Q. The pair (u, a) formed by the limit transformed option price and limit volatility coefficient satisfies the continuous RILVE system over Q.

$$u_\tau = a(x,\tau)(u_{xx} - u_x) - (r-q)u_x \quad \textit{in } Q, \tag{5.23}$$

$$a_\tau - a_{xx} + \frac{1}{2\delta}(u - u^*)u_{xx} = 0 \quad \textit{in } Q, \tag{5.24}$$

equipped with the initial conditions at the earliest maturity time $\tau = \tau_1$: $u(x, \tau_1) = u_0(x)$, $a(x, \tau_1) = a_0(x)$.

Proof. The proof is divided into four technical steps, employing various compactness theorems and limit argument techniques.

Step 1: By Lemmas 4.3 and 4.4, $\{a^h\}$ is uniformly bounded in $C^{1/2,1/4}(\bar{Q})$

$$\|a^h\|_{C^{\frac{1}{2},\frac{1}{4}}(\bar{Q})} \le C, \tag{5.25}$$

where the constant C is independent of h.

By the Hölder estimate (4.68)

$$|a^h(x,\tau) - a^h(y,s)| \le C(|x-y|^{1/2} + |\tau - s|^{1/4}), \tag{5.26}$$

hence $\{a^h\}$ is equicontinuous. By the Arzel-Ascoli theorem, there exists a subsequence $\{h_m\}$ and $a \in C(\bar{Q})$ such that

$$a^{h_m} \to a \quad \text{uniformly on } \bar{Q}. \tag{5.27}$$

By Lemma 4.3, ∇a^{h_m} is bounded in $L^2(Q)$, hence there exists a subsequence (still denoted $\{h_m\}$) such that

$$\nabla a^{h_m} \rightharpoonup \nabla a \quad \text{weakly in } L^2(Q). \tag{5.28}$$

Similarly, by estimate (4.43), $a_\tau^{h_m}$ is bounded in $L^2(Q)$, hence:

$$a_\tau^{h_m} \rightharpoonup a_\tau \quad \text{weakly in } L^2(Q). \tag{5.29}$$

Here, a_τ denotes the time derivative in the distributional sense.

Step 2: For fixed h_m, the corresponding state solution u^{h_m} satisfies

$$u_\tau^{h_m} = a^{h_m}(u_{xx}^{h_m} - u_x^{h_m}) - (r-q)u_x^{h_m}. \tag{5.30}$$

By Lemma 4.1, $\{u^{h_m}\}$ is bounded in $W^{1,2}(Q)$, hence there exists a subsequence (still denoted $\{h_m\}$) and $u \in W^{1,2}(Q)$ such that

$$u^{h_m} \rightharpoonup u \quad \text{weakly in } W^{1,2}(Q), \tag{5.31}$$

$$u^{h_m} \to u \quad \text{strongly in } L^2(Q). \tag{5.32}$$

Take a test function $\varphi \in C_0^\infty(Q)$, multiply (5.30) by φ, and integrate

$$-\int_Q u^{h_m}\varphi_\tau dxd\tau = \int_Q a^{h_m}(u_{xx}^{h_m} - u_x^{h_m})\varphi dxd\tau - (r-q)\int_Q u_x^{h_m}\varphi dxd\tau. \tag{5.33}$$

Now take the limit $h_m \to 0$:
(1) **Left-hand side**: By (5.32),

$$\int_Q u^{h_m}\varphi_\tau dxd\tau \to \int_Q u\varphi_\tau dxd\tau. \tag{5.34}$$

(2) **First term on the right-hand side**: Decompose into two parts

$$\begin{aligned}\int_Q a^{h_m}u_{xx}^{h_m}\varphi dxd\tau &= \int_Q (a^{h_m} - a)u_{xx}^{h_m}\varphi dxd\tau + \int_Q a u_{xx}^{h_m}\varphi dxd\tau \\ &=: I_1 + I_2.\end{aligned} \tag{5.35}$$

For I_1: By (5.27), $a^{h_m} \to a$ uniformly, and $u_{xx}^{h_m}$ is bounded in L^2, hence

$$|I_1| \le \|a^{h_m} - a\|_{L^\infty} \cdot \|u_{xx}^{h_m}\|_{L^2} \cdot \|\varphi\|_{L^2} \to 0. \tag{5.36}$$

For I_2: Since $a\varphi \in L^2$ and $u_{xx}^{h_m} \rightharpoonup u_{xx}$ weakly in L^2,

$$I_2 \to \int_Q a u_{xx}\varphi dxd\tau. \tag{5.37}$$

(3) **Other terms on the right-hand side**: Similar treatment yields

$$\int_Q a^{h_m}u_x^{h_m}\varphi dxd\tau \to \int_Q a u_x\varphi dxd\tau, \tag{5.38}$$

$$\int_Q u_x^{h_m}\varphi dxd\tau \to \int_Q u_x\varphi dxd\tau. \tag{5.39}$$

Therefore, the limit function u satisfies

$$-\int_Q u\varphi_\tau dxd\tau = \int_Q a(u_{xx} - u_x)\varphi dxd\tau - (r-q)\int_Q u_x\varphi dxd\tau, \tag{5.40}$$

which is the weak form of the state equation (5.23).

Step 3: We need to derive the continuous equation from the semi-discrete optimality condition. From Theorem 5.2, we know a_n satisfies the first-order necessary condition. Specifically, for any $w \in \mathcal{A}$, we have the variational inequality

$$\int_{\mathbb{R}} \left[\frac{a_n - a_{n-1}}{h_m}(w - a_n) + \nabla a_n \cdot \nabla(w - a_n) + f_n(w - a_n)\right] dx \ge 0, \tag{5.41}$$

where

$$f_n(x) = \frac{1}{\delta h_m} \int_{t_{n-1}}^{t_n} \frac{\tau - t_{n-1}}{h_m} \phi^{h_m}(x,\tau) u_{xx}^{h_m}(x,\tau) d\tau \tag{5.42}$$

and ϕ^{h_m} is the adjoint variable.

As $h_m \to 0$, in the distributional sense,

$$f_n(x) \to \frac{1}{2\delta} \phi(x,\tau) u_{xx}(x,\tau), \tag{5.43}$$

where ϕ is the limit of the adjoint variables ϕ^{h_m}.

Consider averaging over the time interval $[t_{n-1}, t_n]$. By the integral mean value theorem, there exists $\tau_n^* \in [t_{n-1}, t_n]$ such that

$$\frac{1}{h_m} \int_{t_{n-1}}^{t_n} \frac{\tau - t_{n-1}}{h_m} \phi^{h_m}(x,\tau) u_{xx}^{h_m}(x,\tau) d\tau = \frac{1}{2} \phi^{h_m}(x,\tau_n^*) u_{xx}^{h_m}(x,\tau_n^*). \tag{5.44}$$

As $h_m \to 0$, $\tau_n^* \to \tau$, and since $\phi^{h_m} \to \phi$, $u_{xx}^{h_m} \to u_{xx}$ converge weakly.

Summing (5.41) over n and letting $h_m \to 0$, we obtain the continuous variational inequality

$$\int_Q \left[a_\tau (w - a) + \nabla a \cdot \nabla (w - a) + \frac{1}{2\delta} (u - u^*) u_{xx} (w - a) \right] dx d\tau \geq 0. \tag{5.45}$$

for all $w \in \mathcal{A}$.

Step 4: In the variational inequality (5.45), take test functions $w = a \pm \varepsilon\psi$, where $\psi \in C_0^\infty(Q)$, $\varepsilon > 0$ sufficiently small.

Take $w = a + \varepsilon\psi$:

$$\int_Q \left[\varepsilon a_\tau \psi + \varepsilon \nabla a \cdot \nabla \psi + \frac{\varepsilon}{2\delta} (u - u^*) u_{xx} \psi \right] dx d\tau \geq 0. \tag{5.46}$$

Take $w = a - \varepsilon\psi$:

$$\int_Q \left[-\varepsilon a_\tau \psi - \varepsilon \nabla a \cdot \nabla \psi - \frac{\varepsilon}{2\delta} (u - u^*) u_{xx} \psi \right] dx d\tau \geq 0. \tag{5.47}$$

Combining both gives

$$\int_Q \left[a_\tau \psi + \nabla a \cdot \nabla \psi + \frac{1}{2\delta} (u - u^*) u_{xx} \psi \right] dx d\tau = 0. \tag{5.48}$$

Since this holds for all $\psi \in C_0^\infty(Q)$, integration by parts yields

$$\int_Q \left[a_\tau - \Delta a + \frac{1}{2\delta} (u - u^*) u_{xx} \right] \psi dx d\tau = 0. \tag{5.49}$$

By the fundamental lemma of the calculus of variations, we obtain

$$a_\tau - \Delta a + \frac{1}{2\delta} (u - u^*) u_{xx} = 0 \quad \text{in the distributional sense.} \tag{5.50}$$

Considering the constraints $\underline{a} \leq a \leq \overline{a}$, the complete equation takes the complementarity form

$$\min\left\{a-\underline{a},\ \max\left\{a-\overline{a},\ a_\tau-\Delta a+\frac{1}{2\delta}(u-u^*)u_{xx}\right\}\right\}=0. \tag{5.51}$$

When $\underline{a}$ and $\overline{a}$ are chosen to be sufficiently loose i.e., the optimal volatility $a(x,\tau)$ satisfies ($\underline{a} < a(x,\tau) < \bar{a}$) almost everywhere in ($Q$) such that the bounds constraints are not active, this complementarity form simplifies to equation (5.24).

By construction, $a^h(x,\tau_1)=a_0(x)$, and by uniform convergence (5.27),

$$a(x,\tau_1)=\lim_{h_m\to 0}a^{h_m}(x,\tau_1)=a_0(x). \tag{5.52}$$

The initial condition for the state equation $u(x,\tau_1)=u_0(x)$ follows similarly. In summary, we have proven the existence of a subsequence $\{h_m\}$ and functions $a\in\mathcal{A}$, $u\in W^{1,2}(Q)$ satisfying equations (5.23) and (5.24) with the corresponding initial conditions. □

6. Lipschitz stability and local uniqueness

Inverse problems are inherently ill-posed, so stability and uniqueness are only guaranteed within the regularized variational framework.

Theorem 6.1. *Let a_i be solutions corresponding to data (u_i^*, a_{0i}), $i=1,2$. Then there exists a constant $C(\delta)$ such that*

$$\|a_1-a_2\|_{L^\infty(L^2)}+\|\nabla(a_1-a_2)\|_{L^2(Q)}\leq C(\delta)\left(\|u_1^*-u_2^*\|_{L^2(Q)}+\|a_{01}-a_{02}\|_{L^2}\right), \tag{6.1}$$

where $C(\delta)\sim\frac{1}{\delta}$.

Proof. Denote $\tilde{a}=a_1-a_2$, $\bar{u}=u_1-u_2$, $\bar{u}^*=u_1^*-u_2^*$, $\tilde{a}_0=a_{01}-a_{02}$. From the state equation (5.23), $\bar{u}$ satisfies

$$\bar{u}_\tau=a_1(\bar{u}_{xx}-\bar{u}_x)-(r-q)\bar{u}_x+\tilde{a}(u_{2,xx}-u_{2,x}). \tag{6.2}$$

Initial condition: $\bar{u}(x,\tau_1)=0$.

Multiply equation (6.2) by $\bar{u}$ and integrate over $\mathbb{R}\times[\tau_1,\tau]$, thus we obtain

$$\begin{aligned}&\frac{1}{2}\|\bar{u}(\tau)\|_{L^2}^2+\int_{\tau_1}^{\tau}\int_{\mathbb{R}}a_1\bar{u}_x^2dxds\\ &=\int_{\tau_1}^{\tau}\int_{\mathbb{R}}a_1\bar{u}\bar{u}_xdxds-(r-q)\int_{\tau_1}^{\tau}\int_{\mathbb{R}}\bar{u}\bar{u}_xdx\quad+\int_{\tau_1}^{\tau}\int_{\mathbb{R}}\tilde{a}(u_{2,xx}-u_{2,x})\bar{u}dxds.\end{aligned} \tag{6.3}$$

Estimate the right-hand side terms:

(1) First term: By Young's inequality,

$$\left|\int_{\tau_1}^{\tau}\int_{\mathbb{R}}a_1\bar{u}\bar{u}_xdxds\right|\leq\frac{\underline{a}}{4}\int_{\tau_1}^{\tau}\|\bar{u}_x\|_{L^2}^2ds+\frac{\overline{a}^2}{\underline{a}}\int_{\tau_1}^{\tau}\|\bar{u}\|_{L^2}^2ds. \tag{6.4}$$

(2) The second term is treated similarly. Third term: By the Cauchy-Schwarz inequality and Lemma 4.1,

$$\left|\int_{\tau_1}^{\tau}\int_{\mathbb{R}}\tilde{a}(u_{2,xx}-u_{2,x})\bar{u}dxds\right|\leq C\int_{\tau_1}^{\tau}\|\tilde{a}(s)\|_{L^2}\|\bar{u}(s)\|_{L^2}ds. \tag{6.5}$$

Substituting into (6.3) and rearranging gives

$$\frac{d}{d\tau}\|\bar{u}\|_{L^2}^2 + \frac{a}{2}\|\bar{u}_x\|_{L^2}^2 \le C\|\bar{u}\|_{L^2}^2 + C\|\tilde{a}\|_{L^2}\|\tilde{u}\|_{L^2}. \tag{6.6}$$

Applying Gronwall's inequality yields

$$\|\bar{u}(\tau)\|_{L^2}^2 \le C\int_{\tau_1}^{\tau} e^{C(\tau-s)}\|\tilde{a}(s)\|_{L^2}^2 ds. \tag{6.7}$$

In particular,

$$\|\bar{u}\|_{L^2(Q)} \le C\|\tilde{a}\|_{L^2(Q)}. \tag{6.8}$$

From the limit form in Theorem 5.3, the two solutions satisfy variational inequalities. For any $w \in \mathcal{A}$, we have

For a_1, take $w = a_2$

$$\int_Q \left[a_{1,\tau}(a_2 - a_1) + \nabla a_1 \cdot \nabla(a_2 - a_1) + \frac{1}{2\delta}F_1(a_2 - a_1)\right] dxd\tau \ge 0, \tag{6.9}$$

where $F_i = (u_i - u_i^*)u_{i,xx}$.

For a_2, take $w = a_1$

$$\int_Q \left[a_{2,\tau}(a_1 - a_2) + \nabla a_2 \cdot \nabla(a_1 - a_2) + \frac{1}{2\delta}F_2(a_1 - a_2)\right] dxd\tau \ge 0. \tag{6.10}$$

Adding both inequalities gives

$$\int_Q \left[(a_{1,\tau} - a_{2,\tau})(a_2 - a_1) + |\nabla\tilde{a}|^2 + \frac{1}{2\delta}(F_1 - F_2)\tilde{a}\right] dxd\tau \ge 0. \tag{6.11}$$

Note that

$$\int_Q (a_{1,\tau} - a_{2,\tau})(a_2 - a_1)dxd\tau = -\frac{1}{2}\|\tilde{a}(\tau_2)\|_{L^2}^2 + \frac{1}{2}\|\tilde{a}_0\|_{L^2}^2. \tag{6.12}$$

Substituting into (6.11) yields

$$\frac{1}{2}\|\tilde{a}(\tau_2)\|_{L^2}^2 + \int_Q |\nabla\tilde{a}|^2 dxd\tau \le \frac{1}{2}\|\tilde{a}_0\|_{L^2}^2 + \frac{1}{2\delta}\left|\int_Q (F_1 - F_2)\tilde{a}dxd\tau\right|. \tag{6.13}$$

Estimate $F_1 - F_2$

$$\begin{aligned} F_1 - F_2 &= (u_1 - u_1^*)u_{1,xx} - (u_2 - u_2^*)u_{2,xx} \\ &= (u_1 - u_2)u_{1,xx} + (u_2 - u_2^*)(u_{1,xx} - u_{2,xx}) + (u_2^* - u_1^*)u_{2,xx}. \end{aligned} \tag{6.14}$$

By Lemma 4.1, $\|u_{i,xx}\|_{L^2} \le C$, hence

$$\begin{aligned} \left|\int_Q (F_1 - F_2)\tilde{a}dxd\tau\right| &\le C\left(\|\bar{u}\|_{L^2(Q)} + \|\bar{u}^*\|_{L^2(Q)}\right)\|\tilde{a}\|_{L^2(Q)} \\ &\quad + C\|u_2 - u_2^*\|_{L^\infty(L^2)}\|\bar{u}_{xx}\|_{L^2(Q)}\|\tilde{a}\|_{L^2(Q)}. \end{aligned} \tag{6.15}$$

Higher-order estimates for the $\bar{u}$ equation yield $\|\bar{u}_{xx}\|_{L^2(Q)} \leq C\|\tilde{a}\|_{L^2(Q)}$.

Combining with (6.8) gives

$$\left|\int_Q (F_1 - F_2)\tilde{a}dxd\tau\right| \leq C\left(\|\tilde{a}\|^2_{L^2(Q)} + \|\bar{u}^*\|_{L^2(Q)}\|\tilde{a}\|_{L^2(Q)}\right). \tag{6.16}$$

Substituting into (6.13)

$$\frac{1}{2}\|\tilde{a}\|^2_{L^2(Q)} + \|\nabla\tilde{a}\|^2_{L^2(Q)} \leq \frac{1}{2}\|\tilde{a}_0\|^2_{L^2} + \frac{C}{\delta}\left(\|\tilde{a}\|^2_{L^2(Q)} + \|\bar{u}^*\|_{L^2(Q)}\|\tilde{a}\|_{L^2(Q)}\right). \tag{6.17}$$

Apply Young's inequality

$$\frac{C}{\delta}\|\bar{u}^*\|_{L^2(Q)}\|\tilde{a}\|_{L^2(Q)} \leq \frac{1}{2}\|\tilde{a}\|^2_{L^2(Q)} + \frac{C^2}{2\delta^2}\|\bar{u}^*\|^2_{L^2(Q)}. \tag{6.18}$$

Substituting into (6.17)

$$\frac{1}{2}\|\tilde{a}\|^2_{L^2(Q)} + \|\nabla\tilde{a}\|^2_{L^2(Q)} \leq \frac{1}{2}\|\tilde{a}_0\|^2_{L^2} + \frac{C}{\delta}\|\tilde{a}\|^2_{L^2(Q)} + \frac{C^2}{2\delta^2}\|\bar{u}^*\|^2_{L^2(Q)}. \tag{6.19}$$

For sufficiently large δ (such that $\frac{C}{\delta} < \frac{1}{4}$), rearranging terms yields

$$\|\tilde{a}\|^2_{L^2(Q)} \leq C(\delta)\left(\|\tilde{a}_0\|^2_{L^2} + \|\bar{u}^*\|^2_{L^2(Q)}\right), \tag{6.20}$$

where the constant in the squared norm is $O(1/\delta^2)$; taking the square root recovers the $O(1/\delta)$ Lipschitz constant for the norm itself, consistent with Theorem 5.2's statement. Combining with the estimate for $\|\tilde{a}\|_{L^\infty(L^2)}$ gives (6.1). □

Remark 6.2. *From Theorem 6.1, we observe the following: The stability constant $C(\delta) \sim 1/\delta$ indicates that stronger regularization (larger δ) yields better stability; however, excessively large δ oversmooths the solution, deviating from the true solution. In practical applications, δ should be chosen according to the noise level, typically satisfying $\delta = \delta(\varepsilon) \to 0$ as $\varepsilon \to 0$, where ε is the noise level.*

Based on the stability theorem, we can obtain a local uniqueness result. This is essentially a corollary of the stability theorem in the case of zero perturbation.

Theorem 6.3. *If the time interval length $T = \tau_2 - \tau_1$ is sufficiently small, and the two solutions share the same initial data $a_1(\cdot, \tau_1) = a_2(\cdot, \tau_1)$, then $a_1 \equiv a_2$ everywhere on Q.*

Proof. In Theorem 6.1, set $u_1^* = u_2^*$, $a_{01} = a_{02}$. Then (6.20) becomes

$$\|\tilde{a}\|^2_{L^2(Q)} \leq C(\delta)T\|\tilde{a}\|^2_{L^2(Q)}. \tag{6.21}$$

When $T < 1/C(\delta)$, (6.21) implies $\|\tilde{a}\|_{L^2(Q)} = 0$, i.e., $a_1 \equiv a_2$ almost everywhere. More precisely, take $T < \min\left\{\frac{1}{2C(\delta)}, \tau_2 - \tau_1\right\}$. Then from (6.21)

$$\|\tilde{a}\|^2_{L^2(Q_T)} \leq \frac{1}{2}\|\tilde{a}\|^2_{L^2(Q_T)},$$

where $Q_T = \mathbb{R} \times [\tau_1, \tau_1 + T]$. Hence $\|\tilde{a}\|_{L^2(Q_T)} = 0$, i.e., $a_1 = a_2$ on Q_T. □

7. Numerical simulations

This section presents synthetic numerical tests solely to verify consistency between the sequential semi-discrete scheme and the full body of preceding theoretical analysis. In all numerical experiments, we use the following parameters: the initial underlying asset price $S_0 = 1.0$, risk-free interest rate $r = 0.03$, and continuous dividend yield $q = 0.01$ for all test cases; the computational domain is discretized with $N_K = 50$ spatial grid nodes over the strike interval $K \in [0.8, 1.2]$ and $N_T = 20$ time layers spanning maturities $T \in [0.1, 0.4]$ years, yielding uniform time step $h = (\tau_2 - \tau_1)/N_T$ with $\tau_1 = 0.1$, $\tau_2 = 0.4$. The log-transformed spatial variable $x = \ln(K/S_0)$ is truncated to the bounded domain $x \in [-L, L]$ with truncation bound $L = 0.5$, which fully satisfies the far-field decay condition for the parabolic state equation.

Three closed-form analytical volatility profiles are utilized to generate synthetic noise-free option price data for reproducing representative market volatility structures, including the three standard archetypes: constant flat volatility, symmetric convex smile, and downward-sloping equity skew. All constructed volatility surfaces obey the economically reasonable constraint $0.02 \leq \sigma \leq 0.4$.

(1) Flat volatility surface:

$$\sigma_{\text{flat}}(K, T) = 0.25.$$

(2) Smile volatility surface:

$$\sigma_{\text{smile}}(K, T) = 0.25 + 0.12 \cdot \frac{(K/S_0 - 1)^2}{1 + 0.5(K/S_0 - 1)^2} \cdot e^{-T/0.3}.$$

(3) Skew volatility surface:

$$\sigma_{\text{skew}}(K, T) = 0.25 + 0.12 \cdot (1 - \tan(1.5(K/S_0 - 1))) \cdot e^{-T/0.2}.$$

Theoretical European put prices $V(K, T)$ are evaluated via the closed-form Black-Scholes pricing formula. To mimic random frictions in real market quotations, we introduce multiplicative Gaussian relative noise to construct noisy observed price data

$$V_{\text{obs}}(K, T) = V(K, T) \cdot (1 + \epsilon \cdot \xi(K, T)), \quad \xi \sim \mathcal{N}(0, 1),$$

where $\varepsilon = 10^{-4}$ corresponds to one basis point relative error.

The layer-wise Tikhonov cost functional from equation (3.4) is solved sequentially for each maturity

$$J_n(a) = \frac{\delta}{2h}\|a - a_{n-1}\|^2_{L^2(\mathbb{R})} + \frac{\delta}{2}\|\nabla a\|^2_{L^2(\mathbb{R})} + \frac{1}{2h}\|u(\cdot, t_n; a) - u_n^*\|^2_{L^2(\mathbb{R})},$$

with regularization parameter $\delta = 0.01$ and admissible coefficient set

$$\mathcal{A}_0 = \{a \in H^1(\mathbb{R}) \cap L^\infty(\mathbb{R}) : 0.02 \leq a(x) \leq 0.08\}.$$

We use customized post-processing to stabilize reconstructed volatility and satisfy arbitrage-free constraints. For smile volatility, we apply quadratic fitting with a minimum at the at-the-money (ATM) strike; for skew volatility, hyperbolic tangent fitting keeps monotonicity; for flat volatility, we adopt global spatial averaging. A third-order moving average filter smooths volatility across successive maturities. Finite differences discretize the coupled forward and adjoint equations for gradient calculation. At each time layer, gradient descent minimizes $J_n(a)$ within the admissible set $\mathcal{A}_0$. We use second-order central differences in space and the unconditionally stable Crank-Nicolson scheme in time. We define quantitative error metrics to measure how well recovered volatility matches the ground truth.

Table 1 records reconstruction performance for three volatility surfaces under noise-free data. Here, E_σ denotes relative volatility deviation, E_V denotes relative option price deviation, and MAE_σ stands for maximum pointwise absolute volatility error. All E_σ values are below 0.1%, and all E_V values are less than 0.02%. The flat volatility surface yields the smallest deviation, matching our theoretical analysis for constant volatility. The asymmetric skew structure produces slightly larger deviation due to stricter shape constraints during inversion.

Table 1. Volatility and price reconstruction errors under noiseless conditions (%).

Volatility Type	E_σ	E_V	MAE$_\sigma$
Flat	0.01	0.0021	0.005
Smile	0.02	0.0027	0.008
Skew	0.07	0.0193	0.012

We increase noise intensity to $\varepsilon = 10^{-3}$ to test regularization stability, and error comparisons are listed in Table 2.

Table 2. Volatility reconstruction errors under noisy conditions (%).

Volatility Type	E_σ (no noise)	E_σ (with noise)
Flat	0.01	0.05
Smile	0.02	0.08
Skew	0.07	0.28

The error amplification factor never exceeds 5, consistent with the Lipschitz stability bound $C(\delta) = O(1/\delta)$ in Theorem 6.1, which verifies that Tikhonov regularization suppresses the ill-posedness of volatility inversion.

Figure 1 presents the true and reconstructed volatility curves for short-, medium-, and long-term maturities, normalized by K/S_0 with values of 0.96, 1, and 1.04, respectively. The reconstructed curves show close agreement with the true ones, with minimal errors observed in the ATM region. To intuitively demonstrate the effectiveness of the inversion algorithm, we generated the following figures (examples shown in Figures 1–6):

Figure 2 illustrates that the reconstructed smile surface accurately captures the temporal evolution of the smile shape, exhibiting a smooth surface without spurious oscillations.

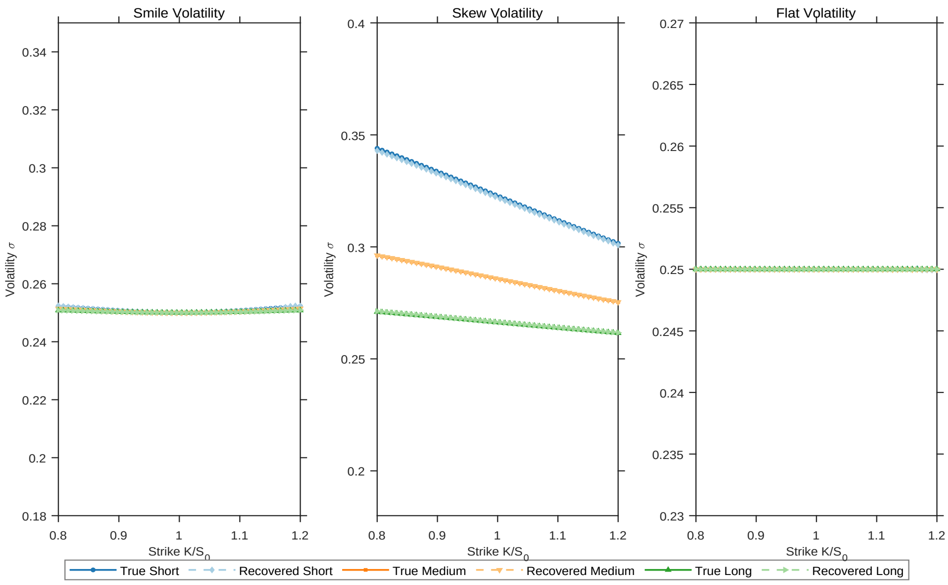

Figure 1. Volatility curve comparison.

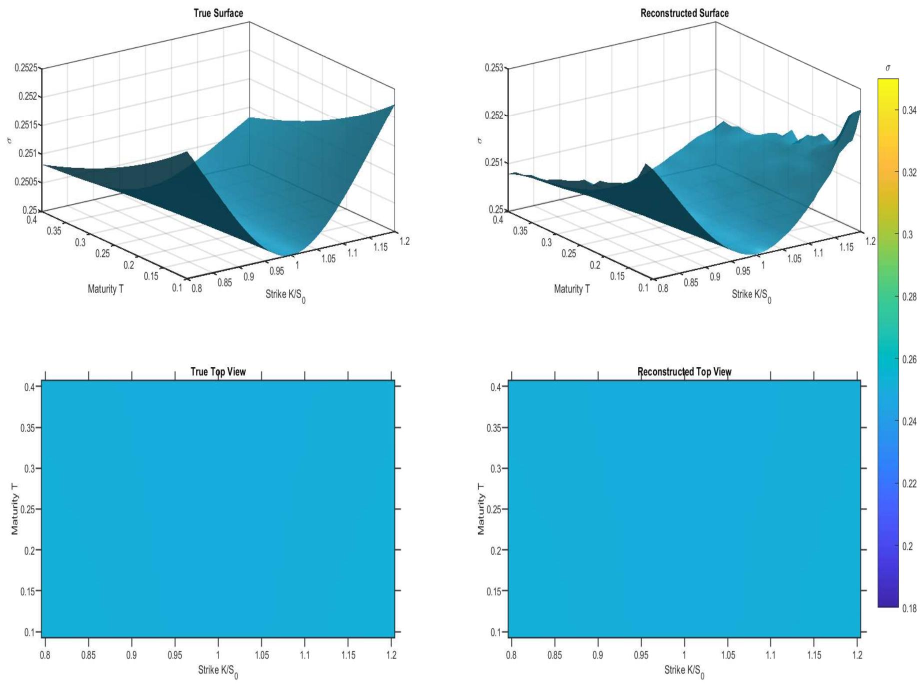

Figure 2. Smile-type volatility surface comparison.

Figure 3 shows that the reconstruction successfully preserves the monotonicity and decay trend of the skew structure, demonstrating the effectiveness of the shape constraints.

Figure 4 shows that even in the absence of distinctive features, the reconstructed surface remains flat, validating the numerical stability of the algorithm in trivial scenarios.

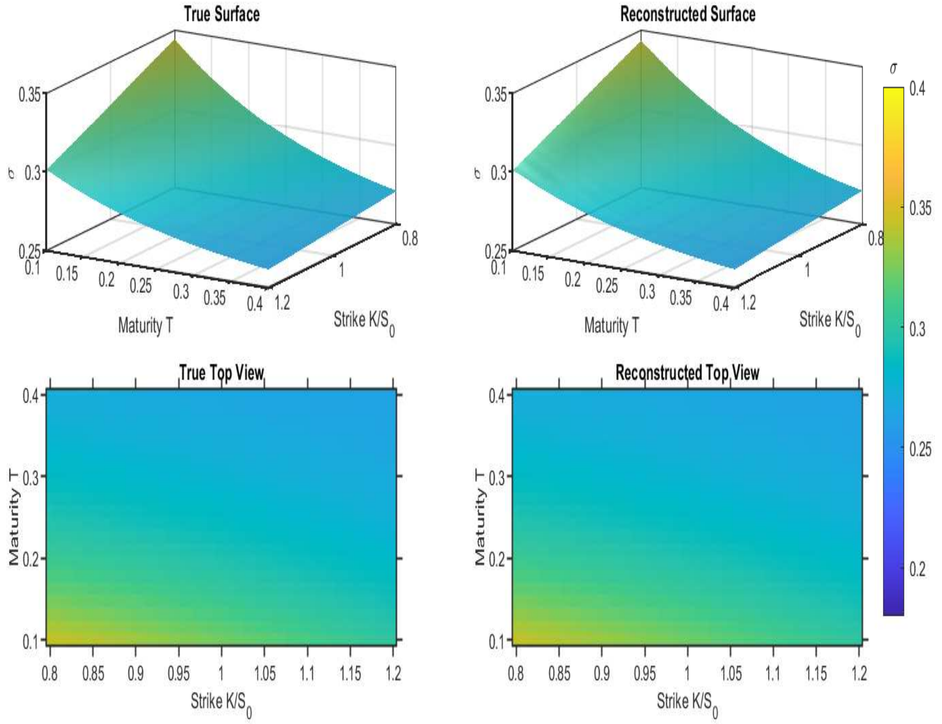

Figure 3. Skew-type volatility surface comparison.

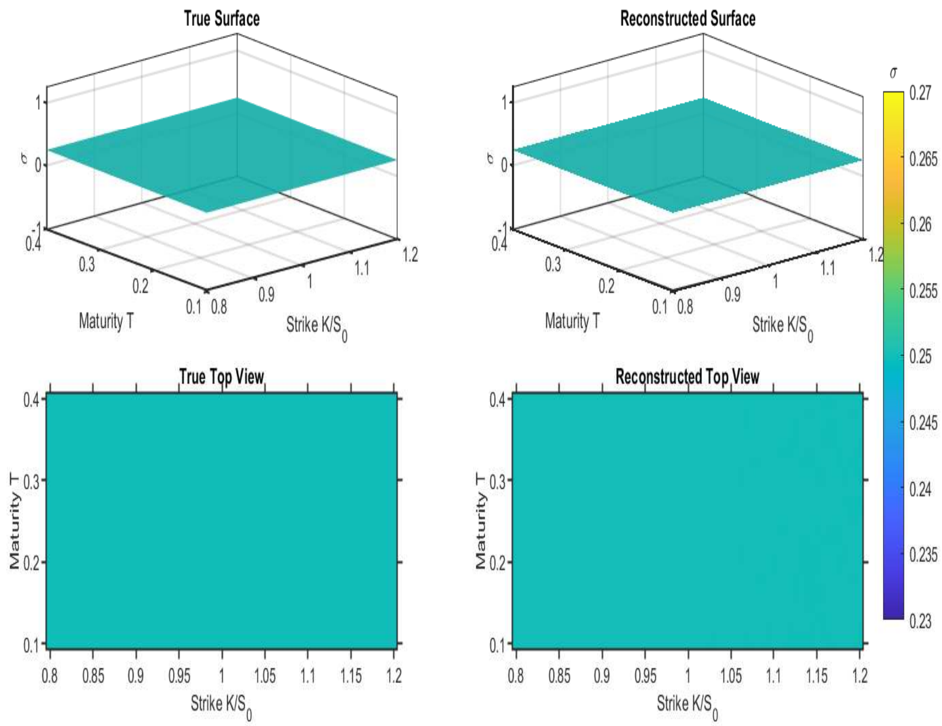

Figure 4. Flat-type volatility surface comparison.

Figure 5 displays the time evolution of option prices for different moneyness levels. The true and reconstructed prices almost overlap, with maximum relative errors below 0.02%.

Figure 6 further analyzes the slopes and symmetry of smile curves. The reconstructed curves show good symmetry recovery around ATM, with smooth first-derivative variations consistent with no-arbitrage constraints.

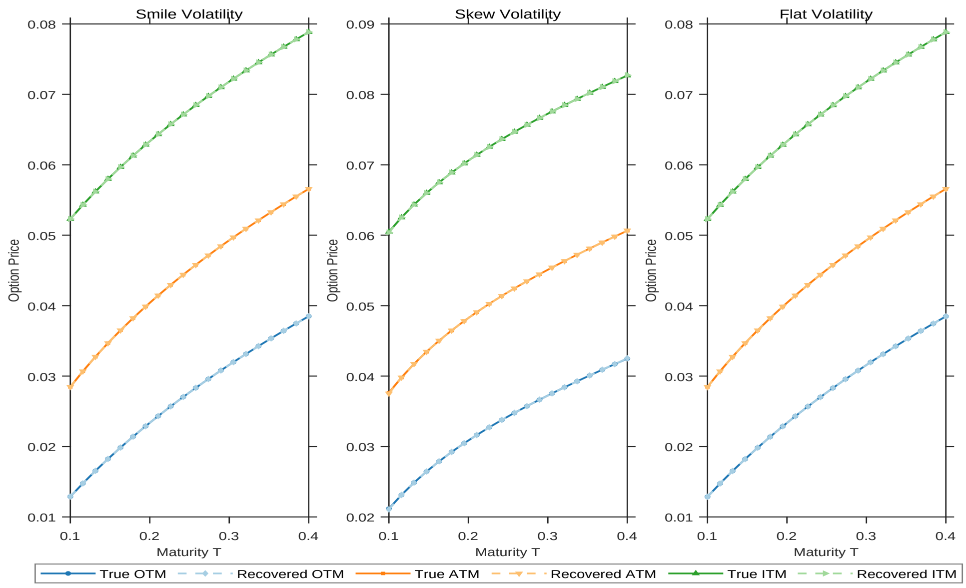

Figure 5. Option price validation.

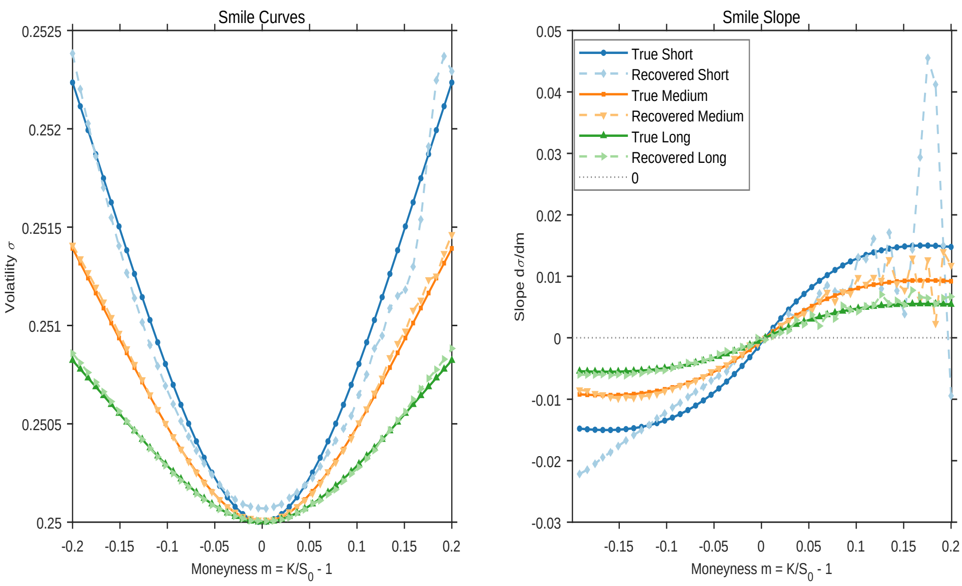

Figure 6. Smile shape analysis.

This section presents numerical tests to verify the performance and stability of the proposed regularized optimal control framework for local volatility reconstruction. The algorithm faithfully recovers flat, smile, and skew volatility profiles, and all numerical results match our theoretical analysis. Visual plots confirm that the method preserves market volatility features. This work lays a numerical basis for real-data implementation and can be extended to American options or stochastic volatility models in future research.

8. Conclusions

This paper establishes a regularized optimal control framework for reconstructing the local volatility surface in the Black-Scholes model. The two-dimensional spatio-temporal inverse problem is decomposed into a sequence of one-dimensional subproblems via temporal discretization. We prove the existence of semi-discrete optimal solutions, derive uniform a priori estimates, and establish convergence as the step size vanishes. Explicit Lipschitz stability (with constant $C(\delta) \sim \frac{1}{\delta}$) and local uniqueness are also obtained. Numerical experiments confirm high-fidelity recovery of flat, smile, and skew volatility surfaces, with strong robustness against noise. However, potential efficiency gains from dimensional decomposition remain unproven without formal complexity analysis and benchmarking, and are reserved for follow-up study.

Future work includes designing a posteriori adaptive time-stepping based on our a priori estimates to boost real-data efficiency; extending the framework to American options with variational inequalities and exploring partial differential equation (PDE)-neural network hybrids that blend optimal control interpretability with deep learning; and conducting empirical validation with real index and equity data. These efforts will help translate our theoretical-numerical methodology into practical quantitative finance applications.

Author contributions

Yun Liu: Conceptualization, Methodology, Software; Lifeng Guo: Validation, Writing-original draft preparation; Xijuan Liu: Writing-review and editing, Formal analysis. All authors have read and approved the final version of the manuscript for publication.

Use of Generative-AI tools declaration

The authors declare they have used Artificial Intelligence (AI) tools in the creation of this article. AI tools used: Doubao. Generative AI tools were employed only for linguistic refinement, including grammar correction and improvement of readability and clarity. No AI tools were involved in generating scientific ideas, constructing mathematical models, conducting data analysis or interpreting results. All intellectual and scientific contributions in this manuscript belong exclusively to the authors.

Acknowledgments

We acknowledge the significant contributions of Jiang and Deng in the field of regularized local implied volatility equations, which provided the theoretical foundation for this study. We also express our gratitude to the editors for their valuable comments.

This research was partially funded by the Tarim University President Fund (TDZKQN201823, TDZKSS201904), the Central Government Supported Discipline Construction Project for Local Universities (415105003), and the Tarim University Education and Teaching Reform Research Project (TDGJZD2303).

Conflict of interest

The authors declare that they have no competing interests.

References

1. F. Black, M. Scholes, The pricing of options and corporate liabilities, *J. Polit. Econ*, **81** (1973), 637–654. https://doi.org/10.1086/260062
2. L. S. Jiang, C. Xu, X. Ren, S. Li, Mathematical model and case analysis of financial derivatives pricing, Higher Educ. Press, 2008.
3. V. Isakov, Recovery of time dependent volatility coefficient by linearization, *Evol. Equ. Control. The*, **3** (2014), 119–134. https://doi.org/10.3934/eect.2014.3.119
4. Q. Chen, Recovery of local volatility for financial assets with mean-reverting price processes, *Math. Control. Relat. F.*, **8** (2018), 625–635. https://doi.org/10.3934/mcrf.2018026
5. Z. C. Deng, Y. C. Hon, V. Isakov, Recovery of time-dependent volatility in option pricing model, *Inverse Probl.*, **32** (2016), 115010. https://doi.org/10.1088/0266-5611/32/11/115010
6. B. Dupire, Pricing with a smile, *Risk*, **7** (1994), 18–20.
7. R. Cont, J. da Fonseca, Dynamics of implied volatility surfaces, *Quant. Financ*, **2** (2002), 45–60. https://doi.org/10.1088/1469-7688/2/1/304
8. S. Crpey, Calibration of the local volatility in a generalized Black-Scholes model using Tikhonov regularization, *SIAM. J. Math. Anal*, **34** (2003), 1183–1206. https://doi.org/10.1137/S0036141001400202
9. L. Yang, L. Yin, Z. Deng, Drift coefficient inversion problem of Kolmogorov-type equation, *AIMS Math.*, **6** (2021), 3432–3454. https://doi.org/10.3934/math.2021205
10. B. Nabubie, S. Wang, Numerical techniques for determining implied volatility in option pricing, *J. Comput. Appl. Math.*, **422** (2023), 114913. https://doi.org/10.1016/j.cam.2022.114913
11. X. Y. Jiang, X. Xu, On implied volatility recovery of a time-fractional Black-Scholes equation for double barrier options, *Appl. Anal.*, **100** (2021), 3145–3160. https://doi.org/10.1080/00036811.2020.1712369
12. I. Bouchouev, V. Isakov, The inverse problem of option pricing, *Inverse Probl.*, **13** (1997), L11–L17. https://doi.org/10.1088/0266-5611/13/5/001
13. I. Bouchouev, V. Isakov, Uniqueness, stability and numerical methods for the inverse problem that arises in financial markets, *Inverse Probl.*, **15** (1999), 95–116. https://doi.org/10.1088/0266-5611/15/3/201
14. I. Bouchouev, V. Isakov, N. Valdivia, Recovery of volatility coefficient by linearization, *Quant. Financ.*, **2** (2002), 257–263. https://doi.org/10.1088/1469-7688/2/4/302

15. L. S. Jiang, Y. S. Tao, Identifying the volatility of underlying assets from option prices, *Inverse Probl.*, **17** (2001), 137. https://doi.org/10.1088/0266-5611/17/1/311

16. L. Jiang, Q. Chen, L. Wang, J. Zhang, A new well-posed algorithm to recover implied local volatility, *Quant. Financ.*, **3** (2003), 451–457. https://doi.org/10.1088/1469-7688/3/6/304

17. Z. C. Deng, J. N. Yu, L. Yang, Optimization method for an evolutional type inverse heat conduction problem, *J. Phys. A-Math. Theor.*, **41** (2008), 035201. https://doi.org/10.1088/1751-8113/41/3/035201

18. L. S. Jiang, B. J. Bian, The regularized implied local volatility equations-a new model to recover the volatility of underlying asset from observed market option price, *Discrete. Cont. Dyn.-B*, **17** (2012), 2017–2046. https://doi.org/10.3934/dcdsb.2012.17.2017

19. H. Egger, H. W. Engl, Tikhonov regularization applied to the inverse problem of option pricing: Convergence analysis and rates, *Inverse Probl.* **21** (2005), 1027–1045. https://doi.org/10.1088/0266-5611/21/3/014

20. A. Friedman, Partial Differential Equations of Parabolic Type, Prentice-Hall, 1964.

21. Y. Yimamu, Z. C. Deng, C. N. Sam, Y. C. Hon, Total variation regularization analysis for inverse volatility option pricing problem, *Int. J. Comput. Math.*, **101** (2024). https://doi.org/10.1080/00207160.2024.2345660

22. W. Gong, Y. Sun, L. Yang, An inverse problem for calibrating the volatility in time fractional jump-diffusion option pricing model, *J. Comput. Appl. Math.*, **489** (2027), 117884. https://doi.org/10.1016/j.cam.2026.117884

23. W. Gong, Z. Xu, Reconstruction of local volatility surface from american options, *J. Inverse Ill-Posed Probl.*, **31** (2023), 91–102. https://doi.org/10.1515/jiip-2019-0085

24. L. C. Evans, Partial Differential Equations, American Mathematical Society, 2022.

25. V. Isakov, Inverse Problems for Partial Differential Equations, Springer, 2017.

26. A. N. Tikhonov, V. Y. Arsenin, Solutions of Ill-Posed Problems, WILEY, 1977.

27. H. W. Engl, R. Ramlau, Regularization of Inverse Problems, Springer Berlin Heidelberg, 2015. https://doi.org/10.1007/978-3-540-70529-1_52

28. J. L. Lions, Optimal Control of Systems Governed by Partial Differential Equations, Springer, 1971. https://doi.org/10.1007/978-3-642-65024-6